

# The final plunge of spinning binary black holes

J. Baker,<sup>1</sup> M. Campanelli,<sup>2</sup> C. O. Lousto,<sup>2</sup> and R. Takahashi<sup>3</sup>

<sup>1</sup>*Laboratory for High Energy Astrophysics, NASA Goddard Space Flight Center, Greenbelt, Maryland 20771*

<sup>2</sup>*Center of Gravitational Wave Astronomy and Department of Physics and Astronomy,  
The University of Texas at Brownsville, Brownsville, Texas 78520*

<sup>3</sup>*Theoretical Astrophysics Center, Dk-2100 København Ø, Denmark*

(Dated: May 22, 2019)

We present the results of the full numerical computation of the gravitational radiation generated by the evolution of a series of binary black hole configurations with aligned and counter-aligned spins,  $s$ , with the orbital angular momentum from near the innermost stable circular orbit (ISCO) down to the final single rotating black hole. While nonspinning binary black holes lead to a final Kerr hole with rotation parameter  $a/M \approx 0.72$ , for the moderate spinning holes studied in detail here the remnant Kerr black formed at the end of an inspiral process have a rotation parameter  $a/M \approx 0.72 + 0.32(s/m_H)$ , suggesting it is difficult (though not excluded) to end up with near maximally rotating holes from such scenarios. The resulting waveforms have still the same qualitative simple appearance of the nonspinning binaries, and support the idea that a total mass rescaling of the latter waveforms can produce an approximate description for the spinning binary case.

PACS numbers: 04.25.Dm, 04.25.Nx, 04.30.Db, 04.70.Bw

## I. INTRODUCTION

The coalescence of two black holes of comparable size will provide the most extreme dynamical tests of General Relativity's predictions. Such coalescences are an anticipated outcome of galactic collision and core merger. The first galaxy with binary active galactic nuclei has, recently, been discovered by X-ray observations of NGC 6240 with the Chandra Observatory [1]. Possible evidence of merger events has also been recently presented in radio observations of X-shaped jet morphologies, which may have been produced by a sudden change in the central black hole's spin axis caused by a supermassive black hole - black hole merger [2].

Such systems of supermassive black holes are expected to occur as the products of galactic mergers with masses exceeding  $10^6 M_\odot$ . Some binaries of main sequence stars may eventually evolve into binary black hole systems with masses on the order of  $10M_\odot$ .[3] It is also possible, though less clear, that a substantial number of black holes exist with masses in the intermediate range.[4] Binary black hole systems are among the more likely observable sources of gravitational waves, with stellar scale systems producing radiation in the frequency band of ground based detectors, while the more massive systems will radiate in the band of space-based detectors like LISA. If larger black holes are produced primarily by successive mergers, rather than accretion, then the details of the merger process may also have an impact on the population statistics, particularly the distribution of spins.

We focus on modeling the final moments of a binary black hole merger, which generates the last few cycles of radiation, carrying away a significant fraction of the system's energy and angular momentum. In a previous paper [5] we have studied non-spinning binary black holes (or irrotational binaries, in the language of binary neu-

tron stars). Our goal here is to extend this treatment to deal with moderately spinning holes. While we generically expect collisions of binary systems with significant mass ratios, systems with a mass ratio near unity can be expected to be the strongest emitters of gravitational radiation at a given system mass. The special case of equal masses is thus a good starting point for these studies, and we will restrict to this case here. As we are interested in the dynamics of these systems at their strongest (most non-linear) moment, our model will necessarily require us to solve Einstein's equations numerically in their fully nonlinear form. The results here are thus complementary to previous studies in both the slow-motion weak-field post-Newtonian (PN) approximation, appropriate when the black holes are still far apart[6, 7] and extreme mass ratio treatments based on near-geodesic motion[8, 9].

In formulating a study of strongly interacting, spinning black holes, we should first ask what manner of spins we expect these systems to have at this late stage of their development, and how we will describe them. We will need to provide initial data to represent strongly interacting black holes with spin, which solve the gravitational constraint equations. Initial data for corotational systems of binary black holes[10, 11] has been suggested as particularly well-motivated from a geometrical point of view, being approximately consistent with a helical Killing symmetry. However, it is not clear that this corotational configuration is astrophysically preferred. Even if we consider the scenario where we suppose two black holes have come together by a quasi-adiabatic inspiral, and tidal forces have managed to lock their spins to co-rotation while they are still well separated, it is difficult to justify that this process will continue to determine the spin dynamics all the way down to the Innermost Stable Circular Orbit (ISCO). In fact, the time scale of the tidal forces seems to be much larger than the orbital one at the end of the quasi-adiabatic motion during the transition

from slow inspiral to plunge [12]. In this scenario, one expects black holes to have some non-vanishing values of the spin at the plunge, but yet smaller than that corresponding to co-rotation at the ISCO. Cook et al [13] have also studied sequences of black holes in circular orbits, on the assumption that the individual black hole spins are not strongly affected by interactions, and thus remain constant through the orbital dynamics. For both types of data, circular orbits, and an ISCO, can be identified by, minimizing the energy of the system at a fixed separation. The results of Ref. [10] agree reasonably well with the corresponding PN ISCO calculations.[6, 7, 14].

In this paper, we adopt the viewpoint that the individual black hole spins vary only slowly as the system approaches the ISCO. In general then, we expect pairings of black holes near ISCO with arbitrary spins. Our focus is on the special case of spins either aligned or anti-aligned with the orbital angular momentum so that we will see only the non-precessional effects of the strong field spin interactions. We apply the Lazarus approach to treat several systems with moderate spin, allowing us to calculate plunge waveforms as well as radiative loss of energy and angular momentum. In the discussion we pay particular attention to how this addition of spin to the problem affects resulting angular momentum of the finally produced black hole.

This paper is organized as follows: Sec. II introduces the Lazarus model of the plunge of binary black holes. Sec. III reports the results of the evolution of spinning holes, and in Sec. IV discuss the implications of these results.

## II. THE MODEL

The goal of the Lazarus approach is to exploit a broad range of analytic and numerical techniques to model black hole binaries during the different stages of the coalescence. In particular, while the Close Limit (CL) approximation Ref. [15, 16] can describe the ring-down of the finally formed black hole, Numerical Relativity (NR) simulations are needed in order to provide a description of the system in the strong non-linear merger stage of the collision. We also need a description for the system applicable in the Far Limit (FL) which can provide initial values for the NR simulations. In this paper we will apply the same CL and NR treatments which we used to study the nonspinning case [5, 17, 18, 19], but we must modify the FL model to allow spinning black holes.

### A. NR and CL treatments

In the present case our simulations are limited to be accurate for less than  $15M$  in time. Making use of adapted “fisheye” coordinates, our spatial domain extends across about  $70M$ , so that we can avoid the delicate issue of

modeling the boundary by ignoring the regions of space-time in the causal future of the boundary.

After evolving for some time we must extract data from the simulation and reinterpret this as a newly forming black hole plus some distortions. We locate the background black hole through a combination of coordinate-based and gauge invariant analysis of the numerical simulation results. Its mass and angular momentum are determined from those of the initial data compensated for radiative losses. A detailed description of our techniques is given in Ref. [18]. We pass the information about this newly formed black hole and its remaining distortions, including any radiation, to be further evolved via the Close Limit treatment. The Close Limit is handled by Teukolsky Kerr black hole perturbation theory. The distortions are represented by a single complex Weyl scalar  $\psi_4$  which evolves according to a 2+1 dimensional linear wave equation (making use of the axial symmetry of the Kerr background we decompose  $\psi_4$  into  $e^{im\varphi}$  modes). The waves propagate away from the strong field region into the wave zone, where  $\psi_4$  provides a description of the gravitational radiation waveform.

### B. FL treatment and initial data

We require some FL model for the spacetime prior to merger, out of which to produce initial data for the NR treatment. Although the inspiral phase of the binary black hole coalescence can be treated with Post-Newtonian methods and their resummation versions[20], these do not necessarily produce well modeled data for the critical spatial region near the black holes. Other FL approaches are necessary to describe the pre-merger stage of the collision. An interesting attempt to include some information from the post-Newtonian expansion while still modeling the region near the black holes in a promising way has recently been introduced and may lead to models with realistic radiation content.[21]. Quasiadiabatic approximations are also under development[22, 23] and may eventually provide another interesting option. At present though, for systems of moderately spinning black holes, we have the most confidence in the well studied Bowen-York-puncture family of solutions to the constraint equations.

In Ref. [5] we applied the Lazarus method to study the plunge of equal mass, nonspinning binary black holes. Our FL treatment was based on a simple kinematical model derived from a family of solutions to the initial value problem of General Relativity, which are constructed according to the Bowen-York ansatz[24]. In general, this construction can represent black hole configurations with arbitrary positions, momenta and spins. One can identify a subset of this family of initial data configurations by “effective potential” methods[25] to represent circular orbits. By construction, in the nonspinning case, this model is intended not to contain any radiation generated in the FL region and does not take into account any

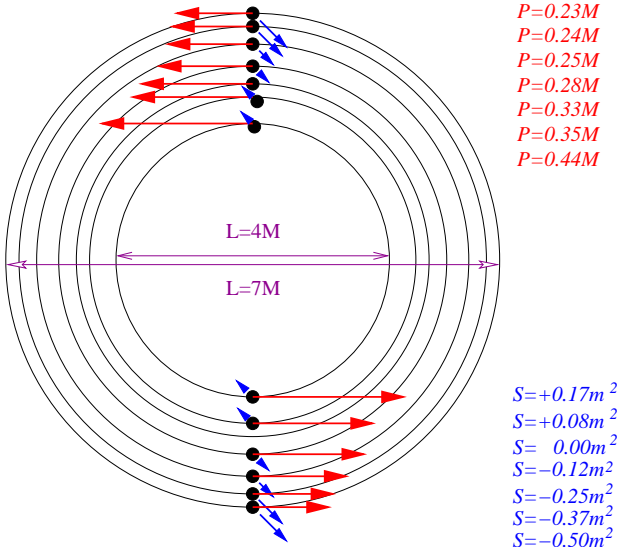


FIG. 1: ISCO configurations of spinning black holes. The horizontal arrow depict the individual black holes' linear momentum,  $P$ , and the arrows going in and out of the page indicate the spins,  $S$ . For spins aligned/anti-aligned with the orbital angular momentum, the repulsive spin-orbit coupling reduces/increases the ISCO separation.

effects of dynamical interaction, but it can be expected to represent a sequence of transient configurations which the system will approximately pass through before coalescence, as long as the holes are sufficiently far apart. The reliability of these data as approximations of real binary black hole system must be assessed dynamically. In Sec.V of Ref. [5] we showed encouraging results suggesting that the plunge waveforms do not depend strongly on the initial separation of black hole within this data family.

We handle spinning black holes in the nearly same way as for the nonspinning case, with the Bowen-York-puncture ansatz [26]. To study plunge radiation we want to begin our simulations with black holes at the innermost stable quasi-circular orbit (ISCO) for *spinning* binary black holes as determined for the Bowen-York-puncture initial data. Various approaches have been developed to compute the location and frequency of the ISCO. We will use results based on the effective potential method of [25] as generalized by Pfeiffer, Teukolsky, and Cook [13] for spinning holes. A sequence of quasi-circular orbit configurations determined by minimizing the binding energy with respect to separation along sequences of constant mass ratio, orbital angular momentum and spin. The ISCO is the limit point of this sequence. We also note that the use of Refs. [13, 25] results, strictly valid for the "image method", holds for the "punctures" since the difference out side the horizons, are very small [27] in practice for the fairly detached black holes studied here.

The parameters of seven ISCO orbits are given in

TABLE I: Spin - ISCO data based on the effective potential method applied to Bowen-York data

$S$	--0.50	--0.37	--0.25	--0.12	++0.00	++0.08	++0.17
$\ell/M$	7.16	6.80	6.29	5.70	5.05	4.70	4.04
$\pm Y/M$	1.930	1.831	1.651	1.433	1.193	1.062	0.810
$\pm P/M$	0.230	0.236	0.254	0.282	0.326	0.356	0.451
$s/M^2$	-0.129	-0.0958	-0.0649	-0.0313	0.00	0.021	0.0449
$J^a/M^2$	0.629	0.672	0.709	0.747	0.779	0.799	0.820
$L^b/M^2$	0.887	0.863	0.838	0.809	0.779	0.757	0.730
$M\Omega$	0.098	0.105	0.118	0.136	0.162	0.182	0.229
$m/M$	0.424	0.448	0.46	0.464	0.455	0.45	0.435
$E_b/M$	-.0159	-.0175	-.0189	-.0208	-.023	-.0250	-.0279

<sup>a</sup>Total: Orbital plus spin

<sup>b</sup>due to orbital motion only

Table I, and Fig.1 provides a comparative illustration. The black holes have parallel spins aligned and counter-aligned with the orbital angular momentum as in Ref. [13]. We label the different cases by  $S$ , the  $z$ -component of each individual black hole's spin, scaled by the square of its mass. This corresponds to the scaled angular momentum parameter  $a/m$  for each hole. In the tables,  $\ell$  represents the proper distance between throats, and  $E_b$  is the binding energy for the given configuration.  $Y$  is the coordinate location of the punctures in conformal space (on the  $y$ -axis),  $P$  is the linear momentum of the holes (as measured from infinity) and are chosen opposite and transversal to the line joining the holes in conformal space, so that for our simulations the total angular momentum,  $J$ , is in the  $z$ -direction. We denote by  $s$  the individual spin of the holes, and  $L$  the orbital angular momentum of the system. The angular frequency of the quasi-circular orbit,  $\Omega$ , is determined from  $dE_b/dL$ . Finally,  $m$  denotes the individual 'puncture' (or bare) masses of the holes, and  $E_b$  is the binding energy for the given configuration. All quantities are normalized to  $M$ , the total ADM mass of the system, and are computed on the initial time slice.

Due to the repulsive nature of the spin-orbit interaction for the '+' cases (spins aligned with the orbital momentum) produce tighter ISCO parameters so they represent, in principle, a more favorable case to be dealt with Lazarus techniques.

The '-' cases (spins counter-aligned with the orbital momentum) have an effective attractive interaction producing hence looser ISCO locations. With the current full numerical techniques we will then be able to deal with those cases that start with not so separated black holes initially.

Note that the Bowen-York initial data family does not have the Kerr limit for larger separations, as the Kerr metric does not have conformally flat slices [28]. Thus,

there will be some extra ‘spurious’ radiation content introduced by the spins. In the far limit, these data describe two distorted Kerr black holes rather than the expected Kerr solutions. Fortunately, for the moderate spins, aligned and anti-aligned with the orbital angular momentum, studied here, this effect can be estimated to be contained below 1% of the radiated energy during the plunge [29]. Thus, to the level of present accuracy, our results are not significantly affected

### III. RADIATION FROM SPINNING BLACK HOLES

In this section we present the results of our simulations beginning from the data described in the last section. As discussed in Ref. [5], we apply several criteria in determining when, or whether, the numerical simulation has ‘linearized’ and close-limit treatment should be applicable. We first look at the values of the  $S$ -invariant, which we expect to be within a factor of two of its background value, unity. We also look for independence in the waveforms on the time  $T$  when we transition from numerical simulation to close limit treatment. In particular, we expect to find independence of the waveform phase for the most significant part of the waveform, as we vary  $T$ . We also expect to see some leveling of the dependence of the total radiation energy as we vary  $T$ , though this tends to be more difficult to achieve. For each case we will determine waveforms, radiation energy and angular momentum, and the state of the final black hole.

#### A. Aligned black holes

##### 1. $SI++0.17$

For this case we are able to run the numerical simulation long enough to numerically locate a common apparent horizon around the black holes. Fig. 2 shows four snapshots of the apparent horizon surfaces [30] on the orbital plane for the  $SI++0.17$  case. The dashed line shows the location of the apparent horizon of the Kerr black hole, which we have identified as the background for the Close Limit calculation. The plots show that the two black holes are well detached at  $T = 0$ . The ‘grid stretching’ effect (due to the vanishing shift we used during full numerical evolution) makes them to grow in the coordinate space. These plots are particularly useful to extract qualitative information about the system. Soon after a common apparent horizon covers the system it tends to have an increasingly spherical shape. The time of formation of a common apparent horizon roughly gives an upper limit to the time at which linear theory can take over as has been discussed in Ref. [18]. It is expected that a common *event* horizon should have appeared some  $M$ ’s of time earlier in the evolution of the system. The key physical feature which actually makes the close limit ap-

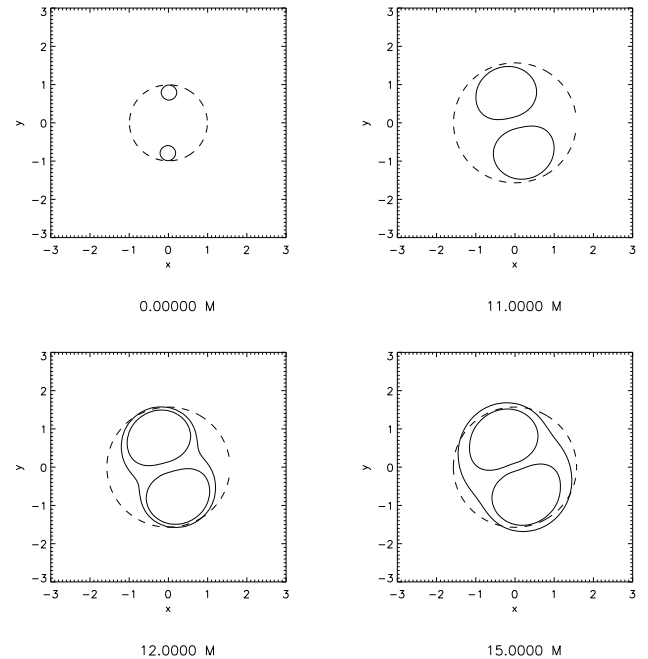


FIG. 2: Apparent horizons for  $SI++0.17$ . The dashed curve indicates the horizon location of the “background” perturbed Kerr black hole, calculated independently.

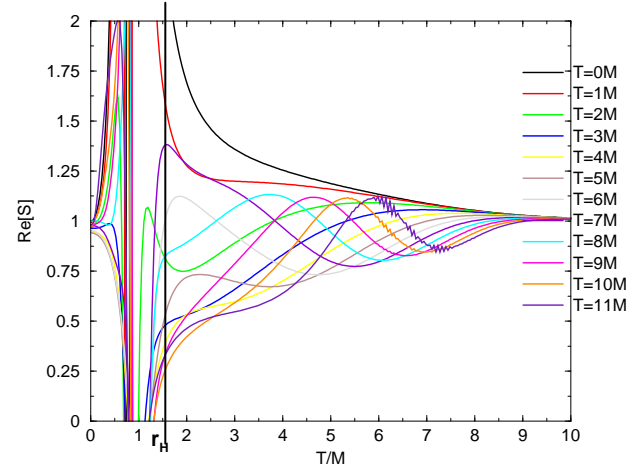


FIG. 3: S-invariant measuring deviations from Kerr for the case  $SI++0.17$  at different full numerical evolution times.

proximation effective is that the black holes share a common potential barrier which appears even earlier than the common event horizon.

Near the time of linearization we estimate the location “background horizon” at  $r_H \approx 1.55$  in the numerical coordinates. In figure 3 we examine the values of the  $S$ -invariant in the vicinity of this horizon. After  $T = 6M$  the  $S$ -invariant outside the horizon seems to be marginally contained within the accepted range for lin-

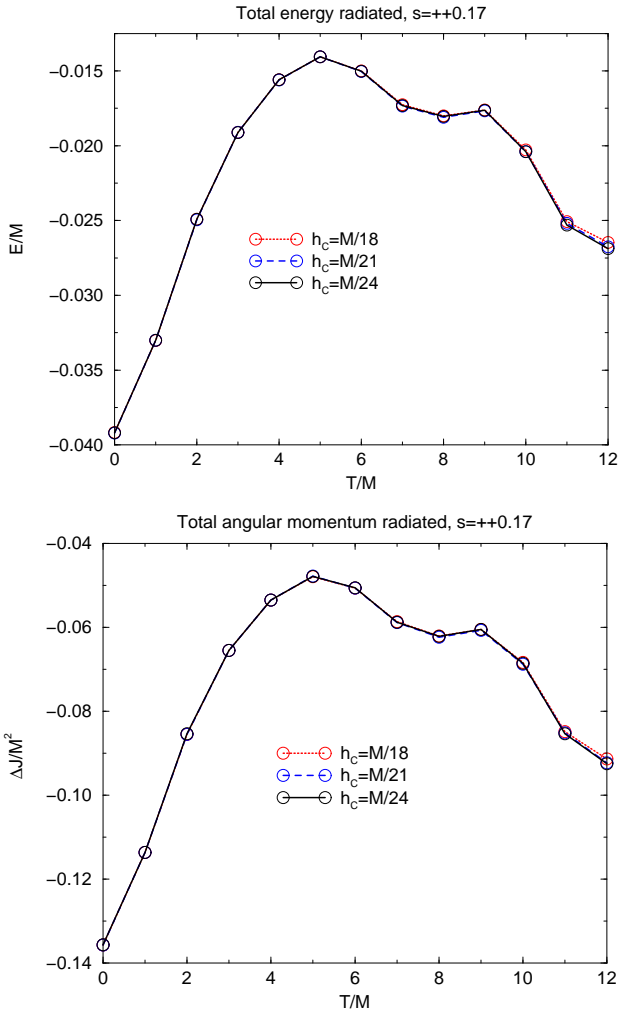


FIG. 4: Energy and angular momentum radiated as a function of the transition time from full nonlinear to linear evolution.

earized theory to take over (roughly speaking  $\text{Re}[S] = 1 \pm 0.5$ , see Ref. [18] for more details). However at  $T = 9M$  and  $10M$  the value is again out of range. This may indicate some persistent non-linear dynamical effect related to the strong field dynamics of close holes.

Figs. 4 for the radiated energy and angular momentum versus time of full nonlinear evolution seems to suggest the beginning of linearization at  $T \approx (7 - 9)M$ , but, again at later times these values drift, this could be a consequence of persistent non-linear dynamics, or a result of mismatching the background black hole. The strong agreement among the several curves corresponding to different resolutions suggest that the renewed growth is not simply a result of numerical error, as we have seen in other cases. On the other hand, the waveforms in the range  $T = 7 - 9M$  already show very strong phase agreement, and the formation of a common apparent horizon already at  $T \approx 12M$  suggests early linearization. This would also agree with the intuition that of the sequence

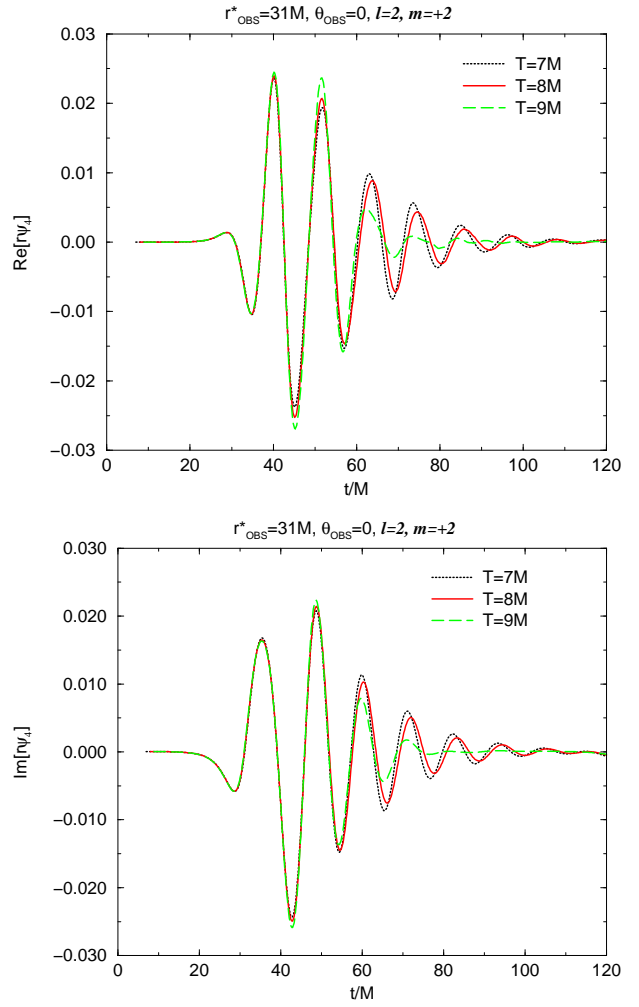


FIG. 5: Waveforms for  $SI++0.17$  in the presumed linear regime for both polarizations.

described in Table I the  $SI++0.17$  case represents the tightest initial configuration.

After two iterations of the background mass and the radiated angular momentum for the final Kerr black hole formed after the plunge we obtain  $M_f \approx 0.982M$  and  $a_f/M_f \approx 0.778$ ; lower than the initial  $J/M^2 = 0.82$ . While the values for taking  $T = 11 - 12M$  results lead to  $M_f \approx 0.975M$  and  $a_f/M_f \approx 0.768$ .

Waveforms during the beginning of linearization show an excellent agreement for up to  $t \approx 65M$  in Fig. 5. Then some lack of superposition in the form of phase or amplitude shift is seen, possibly due to persistent nonlinear effects. The two polarizations represented here by the Weyl scalar  $\psi_4$ , show similar features. The imaginary part of the waveform shows an initial oscillation with a lower frequency component than the corresponding one for the real part of the waveform. This likely has to do with the particular initial configuration we give the black holes, i.e. starting off the  $y$ -axis. We consider this

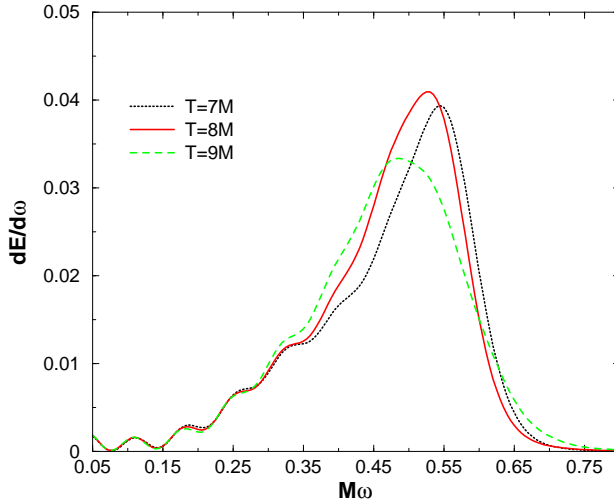


FIG. 6: spectrum for the case  $SI++0.17$  calculated as a sum over all angles and polarizations (for either of the leading modes  $m = \pm 2$ ) in the presumed linear regime.

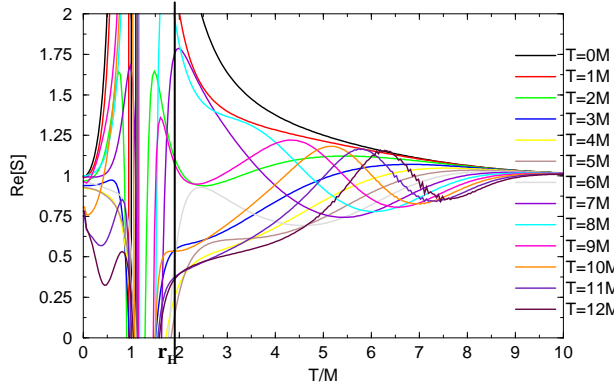


FIG. 7: Snapshots during nonlinear evolution of the S-invariant measuring deviations from a Kerr hole for the case  $SI++0.08$ .

early part of the waveform, say before  $T = 35M$  to be nonphysical, in the sense that it will be directly affected by transient radiation related to the initial data configuration.

We show in Fig. 6 how the amplitude and the location of the maximum of the spectrum (both polarizations added and for the  $m = +2$  mode) depends on the transition time  $T$ . The maximum of the spectrum lies somewhere in  $M\omega = 0.50 - 0.55$ .

## 2. $SI++0.08$

The location of the “background horizon”, near linearization time, in this case can be estimated at  $r_H \approx 1.9$ , in the numerical coordinates. The oscillations of the S-

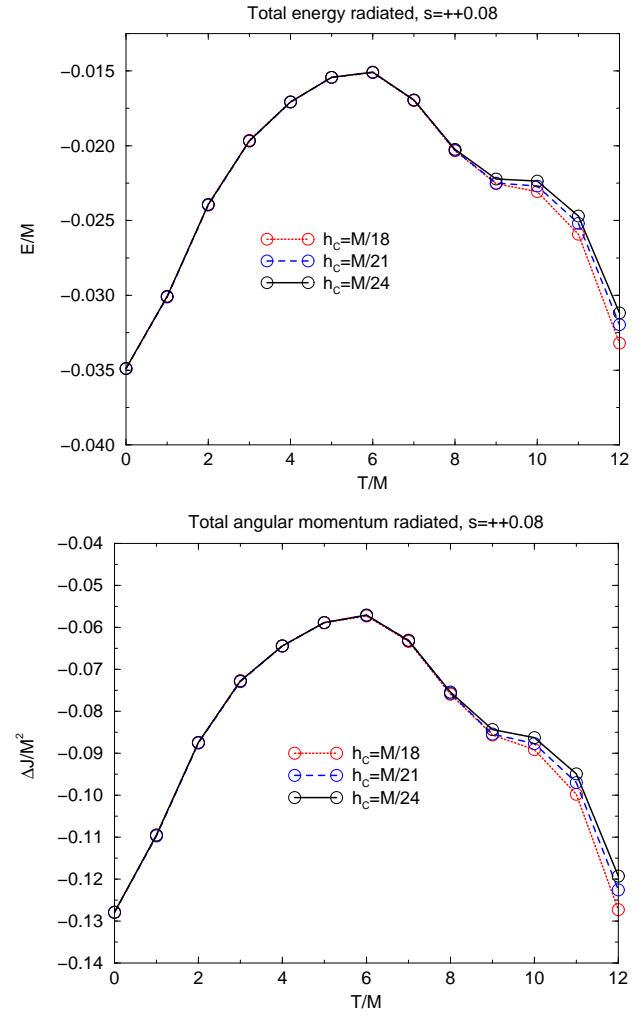


FIG. 8: Energy and angular momentum radiated as a function of the transition time between linear and nonlinear evolution.

invariant show an initial large distortion that damps out as the system evolves. Fig. 7 indicates that after  $T \approx 9M$  a regime is reached that can be handled by perturbation theory.

Fig. 8 displays the radiated energy and angular momentum vs.  $T$  suggesting a linearization time of  $T \approx (9 - 11)M$ . This value agrees with estimates from the S-invariant criteria, shown in Fig. 7.

It is interesting to analyze here the results as a function of the resolution used during full the nonlinear evolution. For  $T \leq 8M$  both the radiated energy and angular momentum curves lie on top of each other for different resolutions. After that time the convergence sequence shows that at low resolutions we are overestimating the radiation produced by the system. An extrapolation of the results to higher resolutions suggest that after  $T \approx 9M$  we reach a sort of stabilization in the values for the radiated energy at around 2.3% – 2.5% and for the loss of angular momentum at around 0.09 – 0.10. Those values are con-

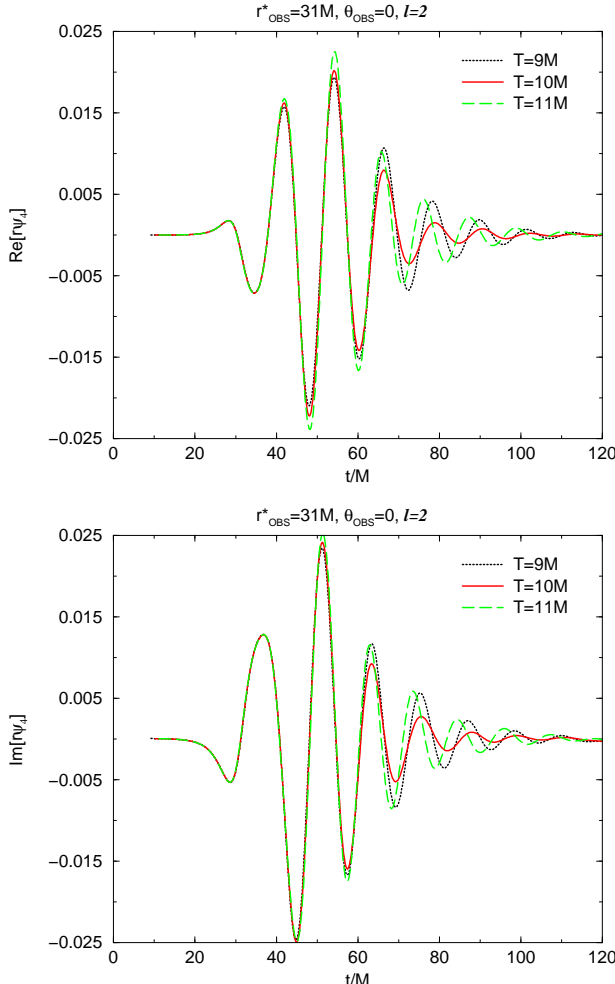


FIG. 9: Waveforms of both polarizations for the  $SI++0.08$  case showing good superposition for  $t < 70M$ .

sistently larger than the previous case,  $SI++0.17$  which agrees with our expectation that from the sequences described in Table I the  $SI++0.08$  case represents the second tightest initial configuration. Note also the increase in the linearization time with respect to the  $SI++0.17$  case.

After two iterations of the background mass and the radiated angular momentum for the final Kerr black hole formed after the plunge we obtain  $M_f \approx 0.977M$  and  $a_f/M_f \approx 0.74$ ; lower than the initial  $J/M^2 = 0.8$ .

The two polarizations of the gravitational radiation, represented by the real and imaginary parts of the Weyl scalar  $\psi_4$ , are shown in Fig. 9, . Good agreement among different transition times is evident for  $t < 70M$ . At later times the waveforms may be affected by effects of the finite location of the numerical boundary and exponentially growing numerical error. Consistent with previous cases the imaginary part of the waveform presents an initial low frequency component followed by a higher frequency one as compared to a more homogeneous real

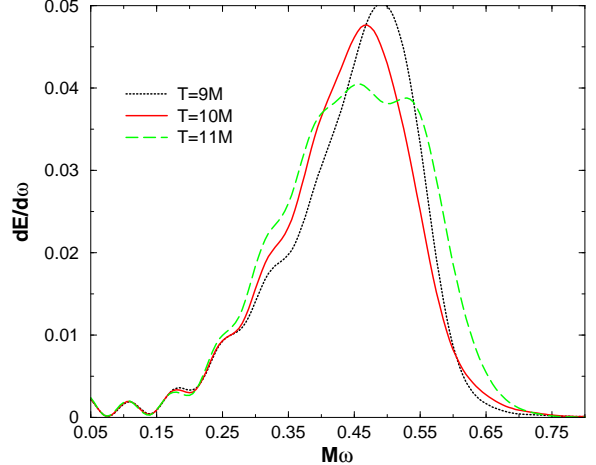


FIG. 10: Total spectrum (for either  $m = \pm 2$ ) for the  $SI++0.08$  case in the presumed linear regime.

part.

The spectra of the two polarizations added for  $m = +2$  at different transition times are displayed in Fig. 10. They also present a single peak and a relatively narrow spectrum with a larger low frequency component compared to the  $SI++0.17$  case. The peak frequency of the spectrum lies somewhere in the  $M\omega = 0.45 - 0.50$  region.

## B. Nonspinning black holes

### 1. $SI++0.00$

We include here a discussion of the non-spinning case, to complete the sequence. This case has been studied more extensively in Ref. [5]. The location of the “background horizon” near linearization time can be estimated in this case at  $r_H \approx 2.0$ , in the numerical coordinates. The oscillations of the S-invariant, show an initial large distortion which damps out as the system evolves reaching a regime that can be handled by perturbation theory after  $T \approx 9M$ .

Figs. 12 suggest a linearization time of  $T \approx (9 - 11)M$ . This values agree with estimates from the S-invariant criteria, as shown Fig. 11.

It is also interesting to observe here the results as a function of the resolution of the full nonlinear evolutions. For  $T \leq 8M$  curves for the energy and the angular momentum radiated for different resolutions lie on top of each. After that time the convergence sequence shows that at low resolutions we are overestimating the radiation produced by the system. An extrapolation of the results to higher resolution suggests that after  $T \approx 9M$  we reach a sort of stabilization in the values for the radiated energy at around 2.5% and for the loss of angular momentum of around 0.10. Those values are consistently larger

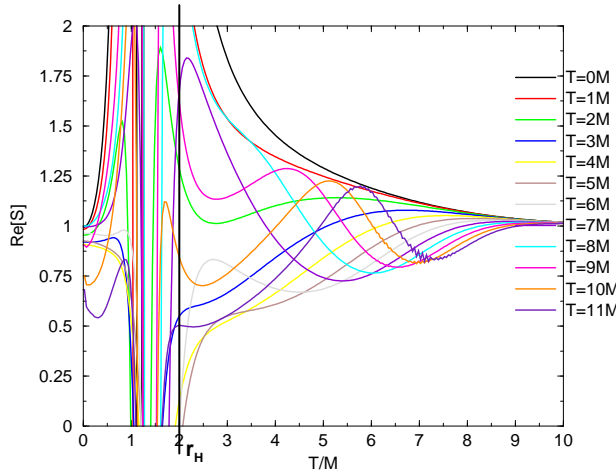


FIG. 11: The S-invariant measuring deviations from Kerr for the non-spinning case shown every  $1M$  of nonlinear evolution.

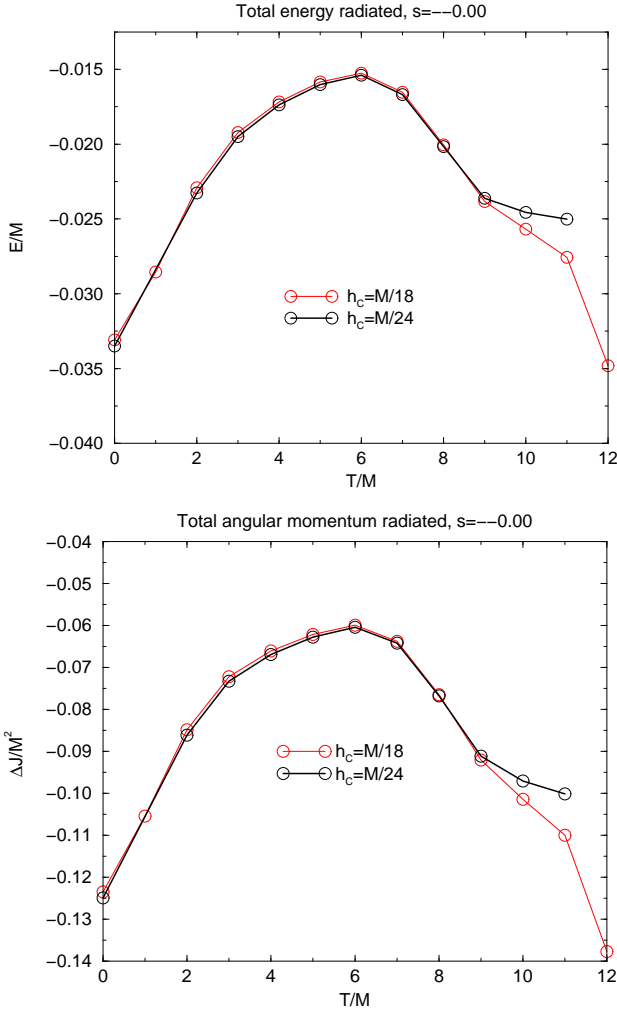


FIG. 12: Energy and angular momentum radiated versus the transition time to switch the evolution from nonlinear to linear.

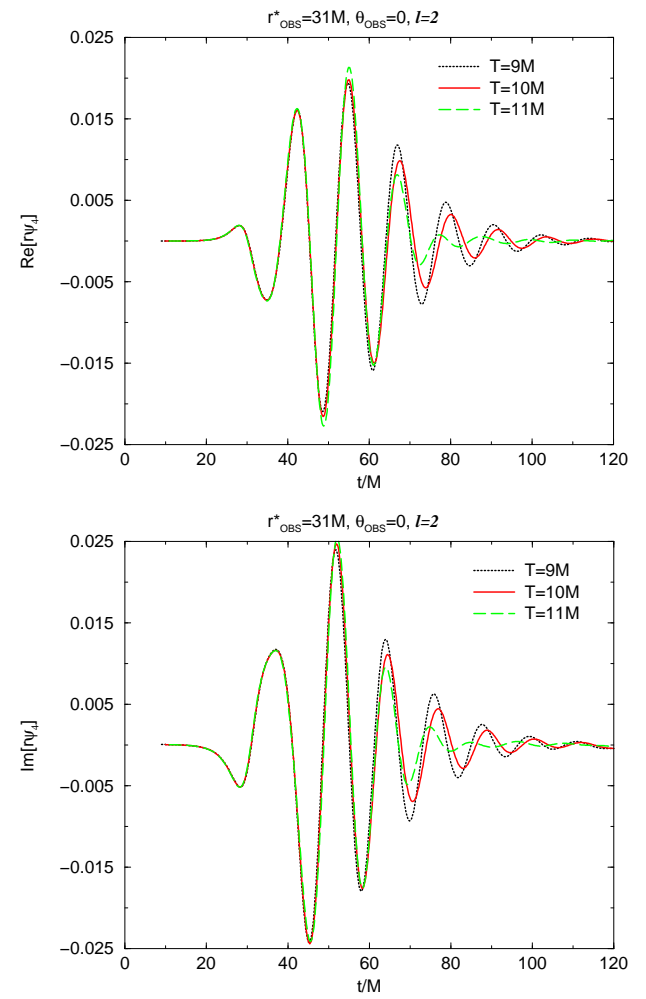


FIG. 13: Waveforms for the non-spinning case  $SI++0.00$ . Both polarizations shown near the linear regime.

than the previous cases,  $SI++0.08$ , and  $SI++0.17$ . Note as well the increase in the linearization time with respect to the  $SI++0.17$  and  $SI++0.08$  cases.

After two iterations of the background mass and the radiated angular momentum for the final Kerr black hole formed after the plunge we obtain  $M_f \approx 0.975M$  and  $a_f/M_f \approx 0.72$ ; lower than the initial  $J/M^2 = 0.78$ .

The two polarizations of the gravitational radiation, in terms of  $\psi_4$ , are shown in Fig. 13, Good agreement among different transition times is evident for  $t < 70M$ . At later times this might be affected by the finite location of the full numerical boundary and exponentially growing numerical error. As with previous cases the imaginary part of the waveform presents an initial low frequency component followed by a higher frequency one as compared to a more homogeneous real part.

The spectra of the two polarizations for  $m = +2$  and different transition times are displayed in Fig. 14. They also present a single peak and a relatively narrow spectrum with a larger lower frequency component compared

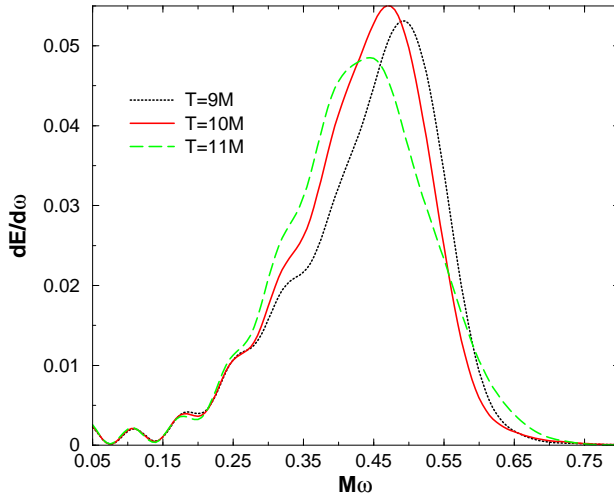


FIG. 14: spectrum for the  $SI++0.00$  case during linearization times.

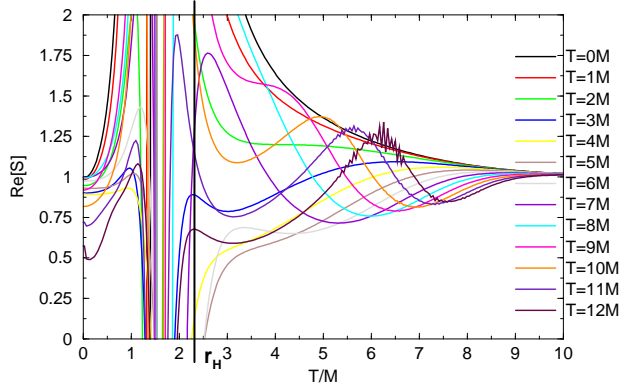


FIG. 15: The S-invariant measuring distortions from the Kerr geometry  $S--0.12$ .

to the  $SI++0.17$  and  $SI++0.08$  cases. The peak frequency lies somewhere in the  $M\omega = 0.45 - 0.50$  region.

### C. Anti-aligned black holes

#### 1. $SI - -0.12$

This case shows larger initial distortions than the cases with parallel spins aligned with the orbital motion. Due to the attractive nature of the effective spin-orbit interaction in this case, the location of the ISCO moves outwards with respect to the non-spinning case. The amplitude of the oscillations of the S-invariant observed in Fig. 15 outside the horizon of the final black hole suggest at least  $T \approx (10 - 12)M$  of full nonlinear evolution are needed for the system to settle down to a single perturbed black hole description. The location of the “background hori-

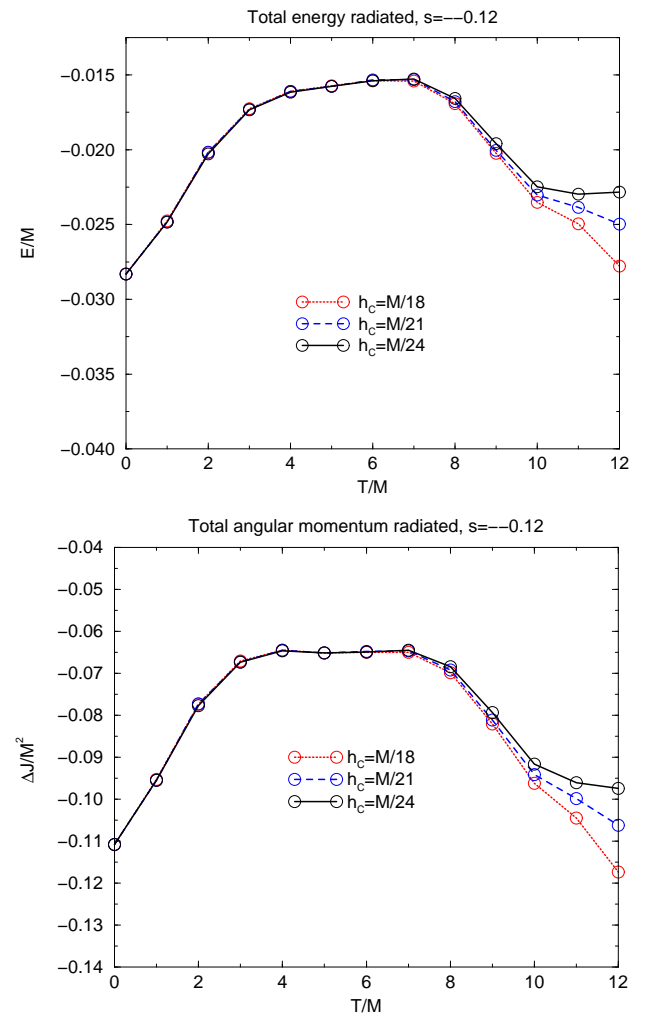


FIG. 16: Energy and angular momentum radiated versus transition time  $T$  for different resolutions showing the plateau indicating linearization for  $T \geq 10M$ .

zon” in this case can be estimated near linearization time at  $r_H \approx 2.3$  in the numerical coordinates.

Figs. 16 suggest a linearization time of  $T \approx (10 - 12)M$  as well. Note the behavior of the energy and angular momentum lost for different resolutions during the full nonlinear phase. For  $T < 8M$  all three runs agree very closely. For later times the trend is clearly towards lower absolute values for both, the radiated energy, just above 2%, and angular momentum radiated around  $-0.09M^2$ . A noticeable relatively flat region in the energy appears for times  $T = 4 - 7M$ , but this is not corroborated by an examination of the waveforms. This is readily discarded as indicating linearization by the other indicators: No common apparent horizon is formed nearly or soon after those times, the S-invariant has still large deviations from 1, and waveforms do not still show any phase locking after  $t \sim 35M$ . We know from Ref. [18] studies that phase locking occurs progressively as we approach the

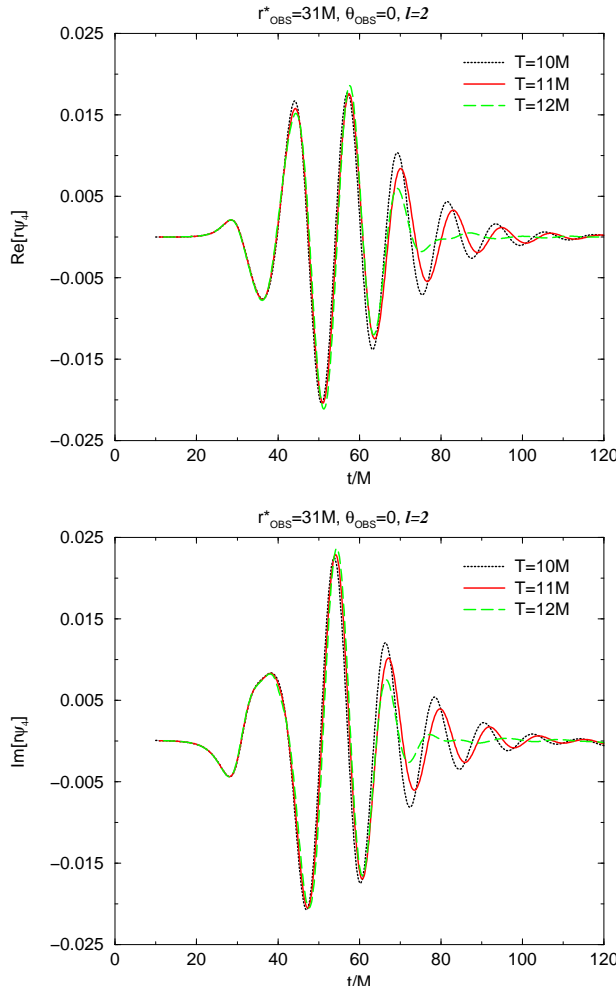


FIG. 17: Waveforms for the case  $SI-0.12$  with good superposition for  $t < 70M$  indicating closeness to linearization.

linearization time by superposing phases from early to later parts of the waveforms.

These values for the linearization time agree with estimates from the S-invariant criteria, Fig. 15. This also agrees with the intuition that of the configurations described in Table I the  $S - 0.12$  case represents the least tight initial configuration studied so far in this paper. Note also the increase in the linearization time with respect to the  $SI+0.17$  and  $SI+0.08$  cases.

After two iterations of the background mass and the radiated angular momentum for the final Kerr black hole formed after the plunge we obtain  $M_f \approx 0.977M$  and  $a_f/M_f \approx 0.68$ , lower than the initial  $J/M^2 = 0.746$ .

Waveforms in Fig. 17 for the real and imaginary parts of  $\psi_4$  display excellent agreement (stressing the consistency of the results) for up to  $t \approx 70M$ . Note that the transition from nonlinear to linear evolution at  $T = 12M$  is clearly contaminated by error from the failure of the full nonlinear code at later times. For transition times  $T = (10 - 11)M$  the agreement is quite good, except for

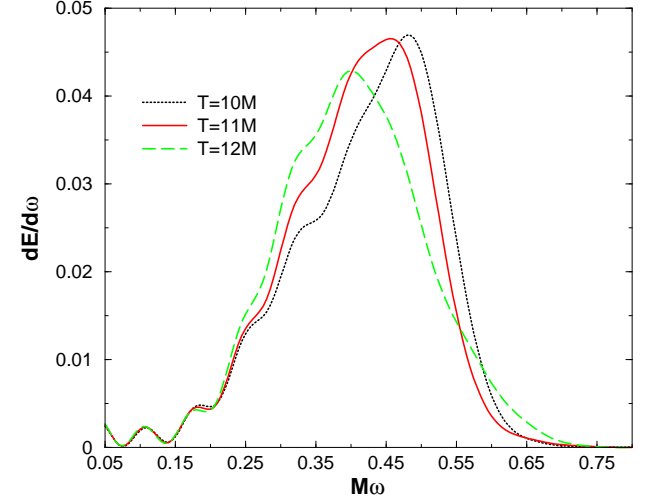


FIG. 18: Total spectrum (for either  $m \pm 2$ ) of the  $SI-0.12$  case near linearization time.

a phase shift at later times. This indicates that we need some more nonlinear evolution to accurately linearize the later part of the waveform while the first half of it has already reached linearization. The same phenomenon has been observed in our previous work [18]. It has to do with the fact that the initial part of the waveform, as seen by an observer far away from the system comes from distortions just outside the potential well, while the later parts of the waveforms come from deeper regions of the dynamical spacetime delayed which take more time to propagate out to a distant observer.

The spectra for three different transition times displayed in Fig. 18 again show a single peak, but with a slightly broader frequency span around  $M\omega \approx 0.40 - 0.50$ . This makes slight shift towards lower frequencies with respect to the previous cases that can be interpreted in terms of contributions coming from the orbital motion and the fact that the system seems to settle down to a final remnant black hole rotating slightly slower than those for the spins aligned with the orbital momentum cases.

## 2. $SI - 0.25$

This case shows the largest initial distortions compared to all the other cases studied in this paper. The location of the ISCO moved further outwards with respect to the previous cases. The amplitude of the oscillations of the S-invariant outside the horizon of the final black hole (shown in Fig. 19) suggest at least  $T \approx (11 - 13)M$  of full nonlinear evolution are needed for the system to settle down to a single distorted black hole description. The location of the “event horizon” in this case can be estimated near linearization time at  $r_H \approx 2.6$  in the numerical coordinates.

Fig. 20 suggests a linearization time of  $T \geq (11 - 13)M$

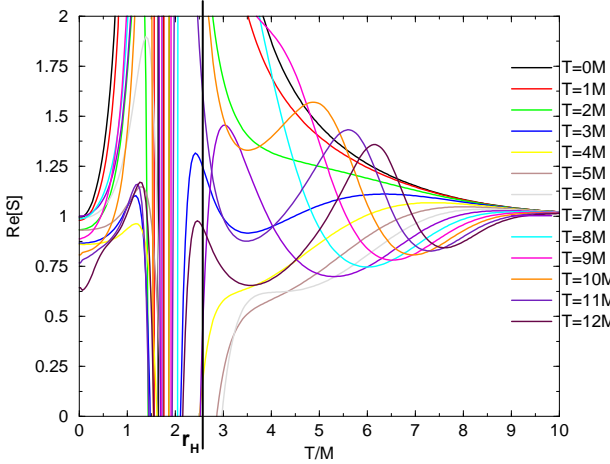


FIG. 19: The S-invariant measuring deviations from the Kerr background for the  $S = -0.25$  case.

as well. Note the dependence of the energy and angular momentum lost by the binary system on grid resolution during the full nonlinear phase. For  $T < 8M$  all three runs agree very closely. For later times the trend is clearly towards lower absolute values for both, the radiated energy, just above 2%, and angular momentum radiated around  $-0.09M^2$ . Again there is a noticeable relatively flat region in the energy for times  $T = (4 - 8)M$ . This time it is interesting to observe that the 'plateau' is not as not as striking in the angular momentum plot. In general there is a strong resemblance in  $T$  dependence of  $E$  and  $J$ . This is a consequence of the strong circular polarization pattern for all waveforms, which imposes the relation  $dE = (\omega/m)dJ$  on the energy and angular momentum carried by the radiation. In this case, further nonlinear evolution, allows lower frequency radiation. Even though the peak amplitude of the waveforms (not shown) and the radiated angular momentum grow with  $T$ , a compensatory decrease in  $\omega$  allows the energy to appear independent. Not surprisingly the other indicators of linearization fail over this range of  $T$  as well. The S-invariant still shows large deviations from 1, and the waveforms do not still show any phase locking at times after  $t \sim 35M$ .

This value for the linearization time  $T \geq (11 - 13)M$  agree with estimates from the S-invariant criteria, Fig. 19. This also agrees with the intuition that from the sequences described in Table I the  $S = -0.25$  case represents the least tight initial configuration studied in this paper. Note also the increase in the linearization time with respect to the  $SI++0.17$ ,  $SI++0.08$ ,  $SI++0.00$ , and  $SI--0.12$  cases.

After two iterations of the background mass and the radiated angular momentum for the final Kerr black hole formed after the plunge we obtain  $M_f \approx 0.977M$  and  $a_f/M_f \approx 0.64$ ; lower than the initial  $J/M^2 = 0.71$ .

Waveforms in Fig. 21 for the real and imaginary parts

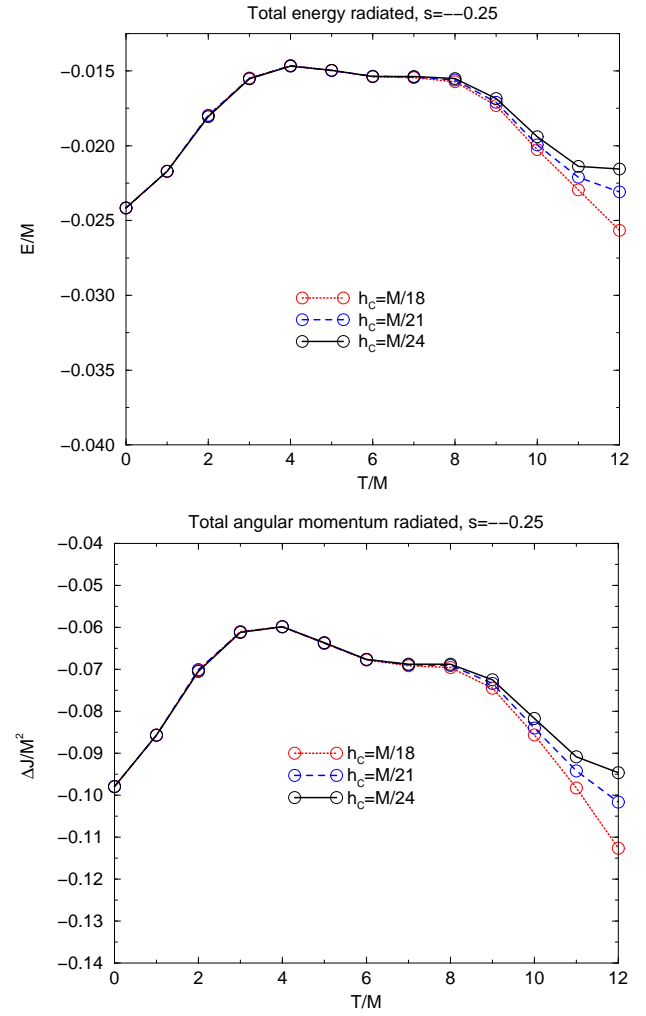


FIG. 20: Energy and angular momentum radiated versus transition for nonlinear to linear evolution for different resolutions of the nonlinear run. A possible plateau suggests itself after  $T = 10M$ .

of  $\psi_4$  display excellent agreement (stressing the consistency of the results) for up to  $t \approx 70M$ . Note that the agreement for transition times  $T = 10 - 12M$  is quite good, except for the phase at later times. We may need a longer nonlinear evolution to accurately linearize the later part of the waveform although the first half of it has already reached linearization.

The spectra for three different transition times displayed in Fig. 22 show a single peak with a slightly broadened frequency span peaked around  $M\omega \approx 0.35 - 0.50$ . It has a slight shift towards lower frequencies with respect to the previous cases that can be interpreted in terms of contributions coming from the orbital motion and from the fact that the system settle down to a final remnant black hole rotating slightly more slowly than those for cases of the aligned spin with the orbital momentum.

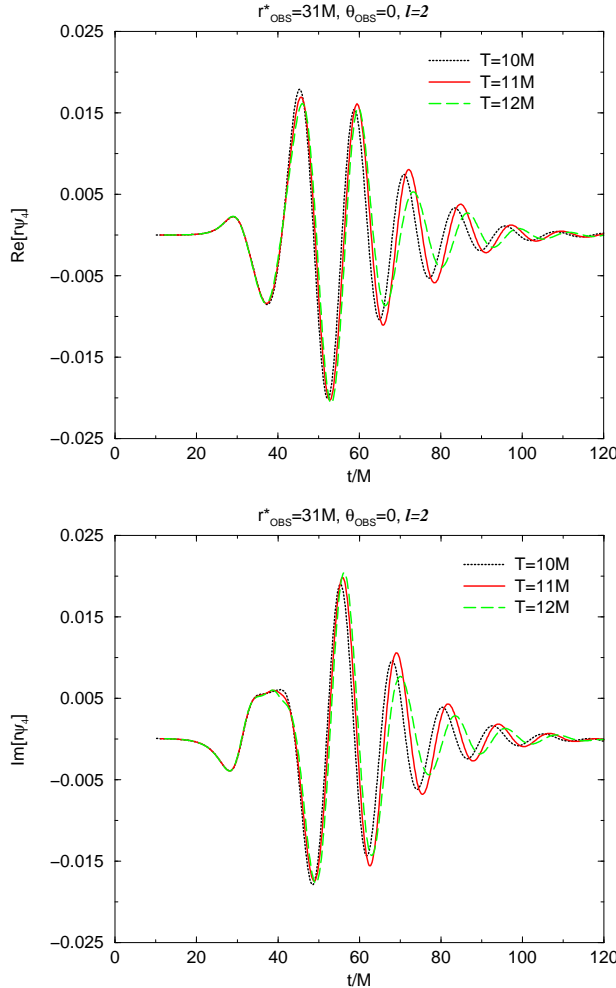


FIG. 21: Waveforms for the  $SI--0.25$  case with good superposition of waveforms in the early part and still a phase shift at later times indicating we are close but not yet at a completely linear regime.

#### D. Critical Assessment

One key element in the Lazarus approach is that it has a built-in self-consistency test associated with the full numerical-close limit and full numerical-far limit interfaces. In the region when either the close or far limits apply together with the full numerics the results should be independent of the transition time chosen to change from one evolution method to the other. The variations in the waveforms near the linearization time suggest that the waveforms follow from the initial data within about 20% accuracy, better for early times and worse for the late ring-down. Nevertheless, in the cases studied here we achieve only a relatively small window where we can perform self-consistency tests. This leaves open the possibility that our results may suffer some systematic error related to underestimated nonlinear effects.

With present technology we are limited by having only

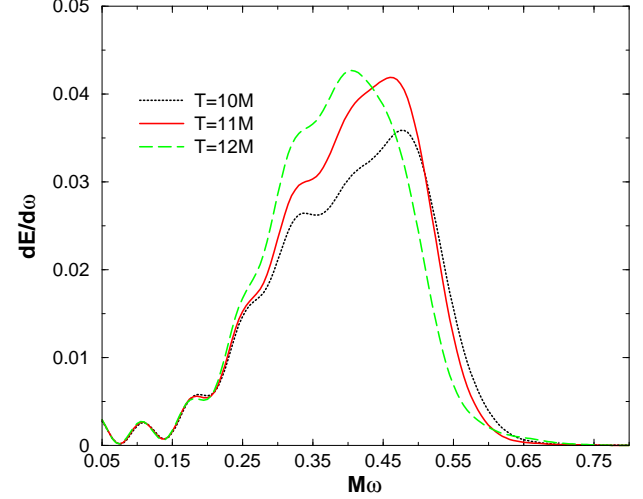


FIG. 22: spectrum for the  $SI--0.25$  case near linearization times

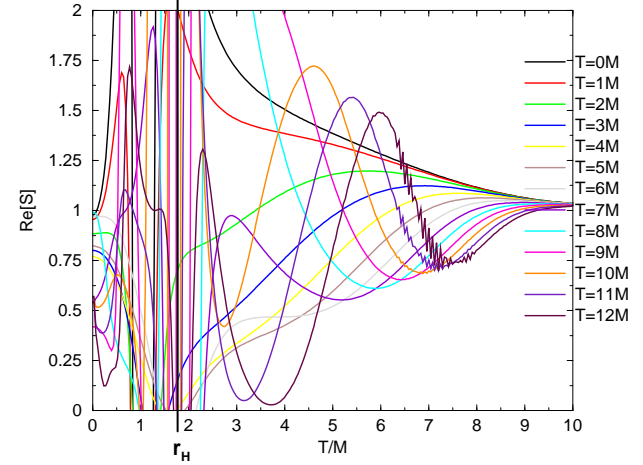


FIG. 23: The  $S$ -invariant measuring deviations from Kerr for  $bbh4$ . The still large amplitude of the outgoing wave indicates that we have not yet reached a linear regime.

$T \sim 12M$  of reliable Full Numerical simulation. This leaves some cases which we would like to study, and which would seem to be nearby in the parameter space of black hole configuration, inaccessible. As an example consider a system of nonspinning black holes with excessive angular momentum. If we increase the linear momentum of ISCO black holes to  $P = 4P_{ISCO}/3$  (labeled as  $bbh4$ ) the initial total angular momentum content of the system is  $J/M^2 = 1.03 > 1$ . We would like to see, in particular, how efficiently the redundant angular momentum is radiated away in order for the system to decay into a single black hole. This system does not seem to form a single black hole before the numerical simulation fails. Fig. 23 shows the  $S$  invariant for this case. With the “event horizon” of the would-be background Kerr hole in

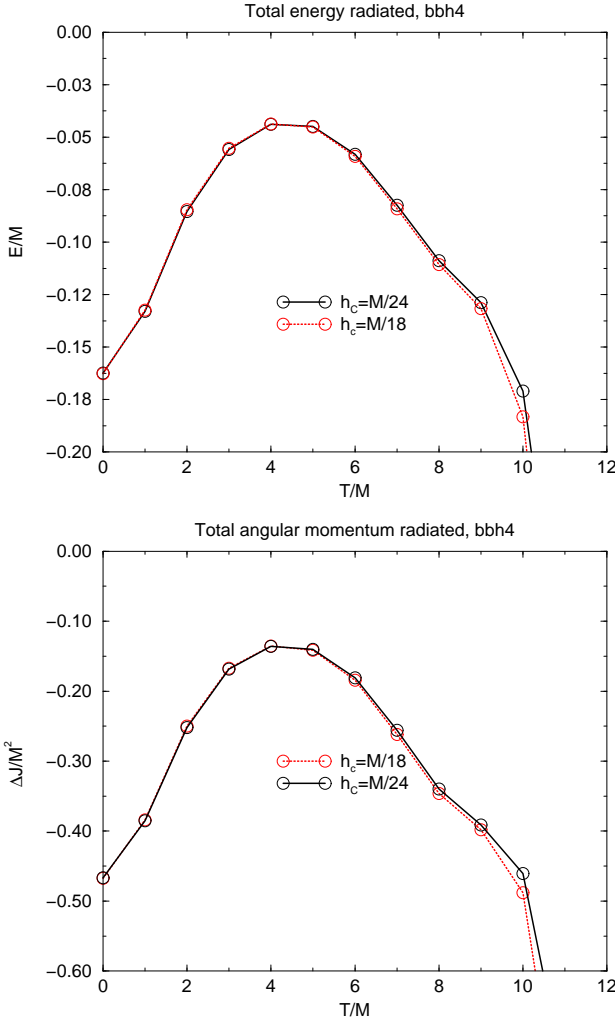


FIG. 24: Energy and angular momentum radiated assuming a single Kerr hole background showing no signs of reaching a linear regime for  $bbh4$ .

this case estimated to lie at  $r_H \approx 1.75$ , it is clear that large distortions remain well outside the horizon even after  $T = 12M$  of evolution. A very large amplitude wave is moving out from the two black holes, and we may need to further evolve some tens of  $M$  in order for the black holes to merge and linearized theory be able to take over. Likewise the waveforms generated by a naive application of our methods show no signs of energy and angular momentum plateaus (see Fig. 24) or phase locking.

Unlike the other cases we have studied, these black holes appear to embark on a significant orbital arc rather than an immediate plunge, thus delaying the formation of a final black hole.

This case serves as an example of when our methods can not be applied with present technology as is readily recognized, standing in stark contrast to borderline cases like the  $SI++0.17$ . In future work we hope to extend the achievable numerical relativity evolution time so

TABLE II: 3PN-ISCO data

Name	$M\Omega$	$E_b/M$	$J/M^2$	$S_i/M^2$
3PN corrot $A(u, \hat{a}^2)$	0.0964	-0.01595	0.888	0.0444
3PN corrot bare	0.0896	-0.0155	—	—
3PN irrot bare	0.1265	-0.01968	0.817	—

that we may be able to treat a broader variety of black hole configurations, like  $bbh4$ . This should also enable the presently treatable and borderline cases to be insensitive to the transition time over a longer period, thereby allowing more definitive waveforms.

The effective potential method, applied to Bowen-York initial data families, identifies a relatively tight innermost stable circular orbit (ISCO) (see entries in table I) compared to the ISCO obtained using 3rd post-Newtonian expansions (see table II). For the sake of comparison we also provide the location of the ISCO as computed using the raw 3PN results of Ref. [31], and those using resummation techniques of Ref. [14].

Note that in Ref. [32] it was stressed that to third post-Newtonian order it is not obvious that the one body resummation is better than the ‘bare’ PN results. For this ‘bare’ case we find that the ISCO so determined have parameters closer to those of Ref. [13].

Notably, table II suggests that going from irrotational configurations to co-rotational ones the ISCO is looser, suggesting attractive interactions between the parallel spins and the orbital angular momentum when they are all aligned. This is in contrast with what was found for the family of initial data studied in Ref. [13]. Notably, this 3PN behavior is also seen in the 2PN results reported in Ref. [32], while Ref. [13] reports good agreement with 2PN results.

In our previous paper [5] we have been able to evolve equal mass, non-spinning binary black hole configurations in quasi-circular orbits corresponding to the 3rd post-Newtonian ISCO (See Fig. 35 there). The resulting waveforms do not differ radically from those evolved from the tighter ISCO parameters determined in Ref. [25]. In fact, the results have been supported by a set of initial data parameters that approximated an evolutionary sequence. We could then determine dynamically the consistency of the results within roughly 20% accuracy as displayed in Fig. 30 of Ref. [5]. Ref. [13], on which we base the cases studied in the present paper, do not contain explicit data for other quasi-circular orbits. Nevertheless, we believe that the current waveforms we obtained for spinning black holes evolved from the ISCO parameters of table I represent a reasonable description of the plunge waveforms for spinning black holes, not strongly dependent on the estimated location of ISCO, from which our simulations begin.

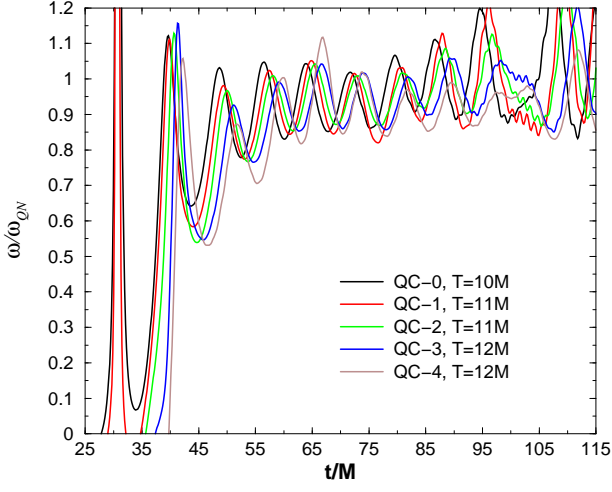


FIG. 25: Time derivative of the phase of the waveforms normalized to quasinormal frequencies of the remnant Kerr hole. This serves as an effective instantaneous frequency for the QC-sequence waveforms showing the approach to the quasinormal frequency. Wiggles in the curves are the effect a small component which is non-circularly polarized component.

#### IV. DISCUSSION OF THE RESULTS

A significant result of our earlier study of nonspinning black hole coalescences was that the waveforms have a relatively simple form. One question we are interested in addressing is whether this simplicity persists when we add spin (but not spin precession) to the problem.

In Ref. [5] the dominant part of the waveform had a circular polarization pattern like that for a rotating body, and with a smoothly increasing frequency (up to the quasinormal ringing frequency) and smoothly varying amplitude. We demonstrated this circular polarization by decomposing our complex  $\psi_4$  waveform into a real amplitude and phase  $\phi$ :  $r\psi_4 = Ae^{i\phi}$ . Because the real and imaginary parts of  $\psi_4$  correspond to the two linear polarization of the gravitational radiation,  $\phi$  is the polarization angle (of radiation along the  $z$ -axis.) After an early period of roughly linear polarization, before the waveforms from the strongly field reach our observation point, the phase increases steadily, indicating circular polarization. Here, rather than plotting  $\phi$  we plot its time derivative  $\omega$ . For circularly polarized radiation  $\omega$  provides a well defined notion of instantaneous frequency. For perfect linear polarization,  $\omega = 0$ , and for a mix it oscillates strongly. As a point of reference we plot in Fig. 25 the circular polarization frequencies for the nonspinning QC-sequence results (obtained in Ref. [5].) We observe an initial rise of the frequency from  $t \sim 33M$  (our observer is located at  $r_{obs}^* \sim 31M$ ) towards the least damped quasinormal frequency. The approach is somewhat delayed for the cases which begin farther apart. Table III provides a summary of the results of evolving

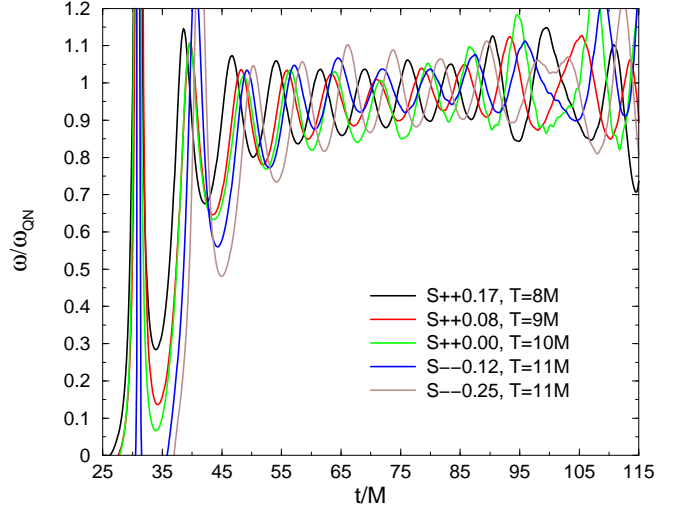


FIG. 26: Instantaneous frequency of waveforms from the coalescence of spinning black holes normalized to quasinormal frequencies of the remnant Kerr holes.

nonspinning black holes for quasicircular orbits located near the ISCO.

Fig. 26 shows the polarization frequencies for the spinning black holes. After we normalize by the final quasinormal ringing frequencies in each case (see Table IV) we see that the quasinormal ringing frequency is approached similarly in each case with a slightly delayed approach for the counter-aligned (--) cases. This is expected for this plunge waveforms since the anti-aligned spin initial data starts with black holes with larger separations than the aligned spin configurations (See Table I). Table IV also gives the least damped quasinormal frequency the final black holes (real  $M\omega_{QN}$ , and imaginary  $M/\tau_{QN}$  parts) from Ref. [33].

The slightly longer timescale in the approach to ring-down is comparable to the slightly longer ring-down wave period. This suggests that we compare the waveforms after a global time rescaling proportional to the ring-down frequency. In Fig. 27 we superpose the waveforms after a rescaling of the time axis by  $q = \omega_{QN}^S / \omega_{QN}^{S=0}$  which corresponds to rescaling by mass in the  $S = 0$  case. We observe a good superposition, particularly in the ring-down region of the waveform. The ring-up, shows some deviations from the quasinormal rescaling, not surprising, since this part of the waveform is more affected by the orbital history of the binary system. This similarity is consistent with the clear trend in the frequency decomposition of the radiation waveforms. From higher mean frequency for the aligned spin configurations to lower frequencies in the anti-aligned cases.

This may amount to an interesting observation for data analysts possibly reducing the parameter space of the search algorithms for binary black hole plunge waveforms by (at least approximately) absorbing variations of one

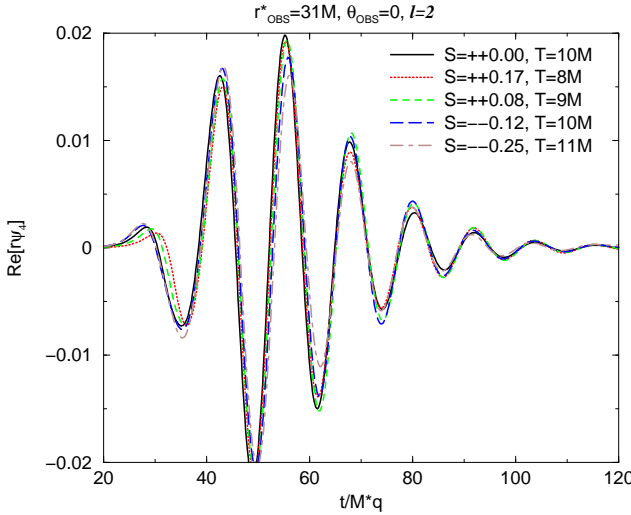


FIG. 27: Rescaling of waveforms by a factor  $q = \omega_{QN}^S / \omega_{QN}^{S=0}$  to show the agreement in the ring-down section.

set of parameters into others [34]. A similar phenomenon has been noted for the inspiral part of binary compact object waveforms. Studies of 2.5PN results[35, 36] show that the inspiral waveforms generated by *spinning* particles can be approximately recovered from the *nonspinning* waveforms by a slight readjustment of the masses. In this case we do something similar, adjusting the timescale by that of the quasinormal ringing frequency.

Aside from the shape of the waveforms, the results from this model allow us to address astrophysical questions about the final state of the black hole formed in the merger. Fig. 28 shows that the initial data for different radii of the quasicircular orbits presents a rather shallow curve in the angular momentum versus initial proper separation plane. This produces a rather robust value of the final Kerr parameter  $a/M \sim 0.72$  consistent with our interpretation that these correspond to the same astrophysical case. (Note that the last two represent border line cases for our current techniques.) The error bars displayed in the figure correspond to taking absolute maximum and minimum of the curves for the radiated energy and the radiated angular momentum versus the transition times (See Fig. 11 in this paper and Fig. 29 of Ref. [5], for instance). While our method gives higher accuracy than this when we reach linearization the current error bars display the robustness of the final results. A curve fitting to the values in the Fig. 28 gives  $J/M^2 \sim 0.779 + 0.0026(L/M - 5) + 0.0038(L/M - 5)^2$  for the initial data and  $a/M \simeq 0.714 + 0.0017(L/M - 5)$  for the final Kerr hole. The case corresponding to a configuration representing a post-Newtonian determination of the ISCO begins with a little more angular momentum, but loses a comparable amount of angular momentum during the plunge.

TABLE III: Quasicircular data for non-spinning black holes

Name	QC-0	QC-1	QC-2	QC-3	QC-4	E1B3PN
$\ell_i/M_i$	4.99	5.49	5.86	6.67	7.84	7.3
$E_b/M_i$	-0.02310	-0.02273	-0.02219	-0.02070	-0.01840	-0.018
$J_i/M_i^2$	0.779	0.781	0.784	0.794	0.817	0.8476
$a_f/M_f$	0.714	0.716	0.715	0.718	0.719	0.752
$M_f/M_i$	0.975	0.975	0.975	0.9725	0.97	0.97
$M_f \omega_{QN}$	0.539	0.540	0.539	0.541	0.542	0.559
$M_f / \tau_{QN}$	0.0802	0.0802	0.0803	0.0801	0.0801	0.0786

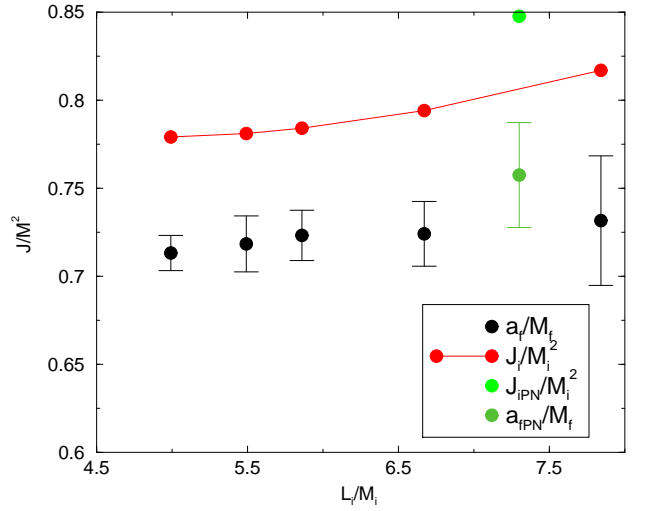


FIG. 28: Rotation parameter for the final Kerr black hole for the QC-sequence showing a weak dependence on the initial configuration.

Table IV summarizes the results of evolving the Spinning-ISCO sequence. We first note a monotonic increase in the linearization times consistent with the increasing radius of the last stable orbit over the range of spin values studied (modulo the uncertain case  $SI++0.17$ ). Nevertheless, the linearization times are small suggesting the holes are directly plunging into each other, for all the initial configurations studied. This is also confirmed by the times of formation of a common apparent horizon which provides a sort of upper limit to the linearization time as discussed in [18]. Regarding the total radiated energy, it seems that a maximum efficiency is reached for the non-spinning case. This probably can be explained by the fact that for aligned spin configurations the ISCO moves inwards reducing the period of nonlinear interaction that generates radiation, while for the anti-aligned configurations there is less total angular momentum to generate radiation.

A particularly interesting quantity derived from each

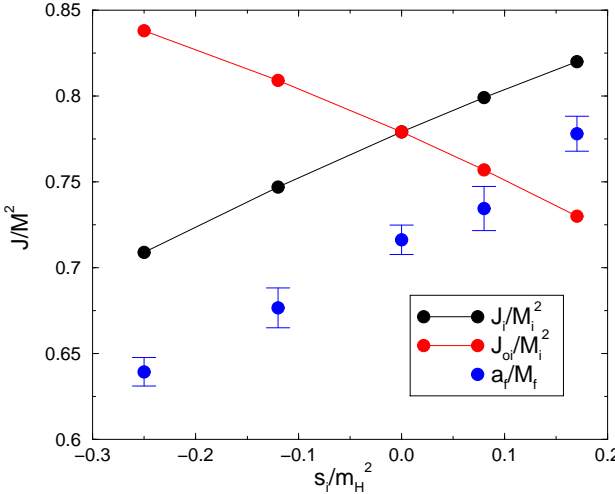


FIG. 29: Rotation parameter for the final Kerr black hole for the Spin-sequence showing a near linear dependence with the initial individual spins normalized to the horizon mass  $s/m_H^2$ .

of these results is the angular momentum parameter for the final remnant Kerr holes formed as a product of coalescence. The remnant black holes have a larger rotation parameter  $a/M$ , for the aligned spin cases than for the anti-aligned ones. In Fig. 29 error bars are estimated by taking the absolute maximum and minimum of the energy and angular momentum radiated versus the transition time as shown in Figs. 4, 8, 12, 16, and 20. This provides us with a much larger error than self-consistency tests suggest, but might be representative of possible systematic errors of our approach.

It is interesting to note here that the rotation parameters of the final Kerr hole  $a_f/M_f$ , of table IV and Fig. 29 are large, but still far from the maximally rotating hole, suggesting it is hard to generate near maximally rotating single holes after the plunge of two inspiraling holes when the have moderate individual rotation parameters like the ones studied in this paper. A curve fitting to the values in the Fig. 29 gives  $J/M^2 \sim 0.779 + 0.2566(s/m_H^2) - 0.0941(s/m_H^2)^2$  for the initial data and  $a/M \sim 0.719 + 0.324(s/m_H^2)$  for the final Kerr hole, where  $m_H$  is the horizon mass of the individual holes and  $s$  its individual spin. If we extrapolate the trend linearly toward  $s/m_H^2 \sim 1$ , the result suggests we would require initially aligned holes with spins  $> 0.85$  in order

to approach a maximally rotating remnant. Our studies thus enhance the conclusions based on complementary studies of binaries in the small mass ratio limit[9] which suggested that it is hard to form a maximally rotating black hole by binary merger unless the mass ratio is near unity. Even in the equal mass case it would seem to take near maximally spinning black holes to produce a maximally spinning remnant. Of course rapidly rotating black holes may still be produced by accretion.

We finally note that we also report the binding energy

TABLE IV: Summary of results for spinning holes

$S$	++0.17	++0.08	++0.00	--0.12	--0.25
$T/M$	7-9	9-11	9-11	10-12	11-12
$-\dot{E}/M(\%)$	1.7-1.9	2.3-2.5	2.4-2.6	1.9-2.1	1.9-2.1
$-\dot{J}/M^2$	0.06-0.08	0.09-0.10	0.09-0.10	0.09-0.10	0.09-0.10
$M_f/M$	0.982	0.976	0.975	0.980	0.980
$a_f/M_f$	0.778	0.739	0.720	0.679	0.639
$J_i/M_i^2$	0.820	0.799	0.779	0.747	0.709
$M\omega_{peak}$	0.50-0.55	0.45-0.50	0.45-0.50	0.40-0.50	0.40-0.50
$M\omega_{QN}$	0.573	0.552	0.542	0.524	0.508
$M/\tau_{QN}$	0.07714	0.07925	0.08006	0.08160	0.08285
$T_{CAH}/M$	12	> 15	> 17	--	--

$E_b$  of the initial configurations in table III for the non-spinning holes and in table IV for the binary spinning holes. If we interpret this binding energy as a measure of the energy radiated in the form of gravitational waves during the whole inspiral period until we reach the initial configuration we use to estimate the plunge radiation, we came to the notable conclusion that approximately as much energy is radiated in the few cycles following the plunge than in the whole history of the binary system.

## Acknowledgments

We thank H.Pfeiffer for making available unpublished data related to Ref. [13]. We also thank the Center for Gravitational Wave Phenomenology (CGWP) in Penn State University (PSU) for hosting a meeting on the subject of this paper. J.B. is supported by the National Research Council. C.O.L and M.C. have financial support from Grants NSF-PHY-0140326 'Kudu' and NASA-URC-Brownsville. The full nonlinear numerical work has been performed in LRZ (Germany) and NERSC (under Contract No. DE-AC03-76SF00098).

---

[1] S. Komossa et al. (2002), astro-ph/0212099, astro-ph/0212099.  
[2] D. Merritt and R. D. Ekers, Science **297**, 1310 (2002), astro-ph/0208001.  
[3] K. Belczynski, V. Kalogera, and T. Bulik (2001), astro-ph/0111452.  
[4] E. Colbert and A. Ptak, *Astrophys. J. Supp.* **143**, 25 (2002), astro-ph/0204002.  
[5] J. Baker, M. Campanelli, C. O. Lousto, and R. Takahashi, *Phys. Rev. D* **65**, 124012 (2002), astro-ph/0202469.  
[6] T. Damour, *Phys. Rev. D* **64**, 124013 (2001), gr-qc/0103018.  
[7] L. Blanchet (2002), gr-qc/0201050, gr-qc/0201050.

[8] M. Saijo, K.-i. Maeda, M. Shibata, and Y. Mino, Phys. Rev. **D58**, 064005 (1998).

[9] S. A. Hughes and R. D. Blandford, Astrophys. J. **585**, L101 (2003), astro-ph/0208484.

[10] P. Grandclement, E. Gourgoulhon, and S. Bonazzola, Phys. Rev. D **65**, 044021 (2001), gr-qc/0106016.

[11] G. B. Cook, Phys. Rev. **D65**, 084003 (2002), gr-qc/0108076.

[12] R. H. Price and J. T. Whelan, Phys. Rev. Lett **87**, 231101 (2001), gr-qc/0107029.

[13] H. P. Pfeiffer, S. A. Teukolsky, and G. B. Cook, Phys. Rev. **D62**, 104018 (2000), gr-qc/0006084.

[14] T. Damour, E. Gourgoulhon, and P. Grandclement, Phys. Rev. **D66**, 024007 (2002), gr-qc/0204011.

[15] R. H. Price and J. Pullin, Phys. Rev. Lett. **72**, 3297 (1994).

[16] C. O. Lousto, Phys. Rev. D **63**, 047504 (2001), gr-qc/9911109.

[17] J. Baker, B. Brügmann, M. Campanelli, and C. O. Lousto, Class. Quantum Grav. **17**, L149 (2000).

[18] J. Baker, M. Campanelli, and C. O. Lousto, Phys. Rev. **D65**, 044001 (2002), gr-qc/0104063.

[19] J. Baker, B. Brügmann, M. Campanelli, C. O. Lousto, and R. Takahashi, Phys. Rev. Lett. **87**, 121103 (2001), gr-qc/0102037.

[20] A. Buonanno and T. Damour, Phys. Rev. **D62**, 064015 (2000), gr-qc/0001013.

[21] W. Tichy, B. Brügmann, M. Campanelli, and P. Diener, Phys. Rev. D **67**, 064008 (2003), gr-qc/0207011.

[22] J. T. Whelan, W. Krivan, and R. H. Price, Class. Quantum Grav. **17**, 4895 (2000), gr-qc/9909076.

[23] M. D. Duez, T. W. Baumgarte, and S. L. Shapiro, Phys. Rev. **D63**, 084030 (2001), gr-qc/0009064.

[24] J. Bowen and J. W. York, Phys. Rev. D **21**, 2047 (1980).

[25] G. B. Cook, Phys. Rev. D **50**, 5025 (1994).

[26] S. Brandt and B. Brügmann, Phys. Rev. Lett. **78**, 3606 (1997).

[27] A. Abrahams and R. Price, Phys. Rev. D **53**, 1972 (1996).

[28] A. Garat and R. H. Price, Phys. Rev. **D61**, 124011 (2000), gr-qc/0002013.

[29] S. Dain, C. O. Lousto, and R. Takahashi, Phys. Rev. D **65**, 104038 (2002), gr-qc/0201062.

[30] M. Alcubierre, S. Brandt, B. Brügmann, C. Gundlach, J. Massó, and P. Walker, Class. Quantum Grav. **17**, 2159 (2000), gr-qc/9809004.

[31] L. Blanchet, Phys. Rev. **D65**, 124009 (2002), gr-qc/0112056.

[32] L. Blanchet (2002), gr-qc/0207037, gr-qc/0207037.

[33] F. Echeverría, Phys. Rev. D **40**, 3194 (1989).

[34] P. Grandclement and V. Kalogera (2002), gr-qc/0211075, gr-qc/0211075.

[35] C. M. Will and A. G. Wiseman, Phys. Rev. **D54**, 4813 (1996), gr-qc/9608012.

[36] E. Poisson and C. M. Will, Phys. Rev. **D52**, 848 (1995), gr-qc/9502040.